Valence, charge transfer, and orbital-dependent correlation in bilayer nickelates $Nd_3Ni_2O_7$

Daisuke Takegami [1,2] Takaki Okauchi [3] Edgar Abarca Morales [2] Koto Fujinuma [1] Mizuki Furo [3] Masato Yoshimura,[4] Ku-Ding Tsuei,[4] Grace A. Pan [5] Dan Ferenc Segedin,[5] Qi Song,[5] Hanjong Paik [6,7,8] Charles M. Brooks [5] Julia A. Mundy [5,9] Takashi Mizokawa [1] Liu Hao Tjeng [2] Berit H. Goodge [2,*] and Atsushi Hariki [3,†]

[1]*Department of Applied Physics, Waseda University, 3-4-1 Okubo, Shinjuku-ku, Tokyo 169-8555, Japan*
[2]*Max Planck Institute for Chemical Physics of Solids, Nöthnitzer Str. 40, 01187 Dresden, Germany*
[3]*Department of Physics and Electronics, Osaka Metropolitan University, 1-1 Gakuen-cho, Nakaku, Sakai, Osaka 599-8531, Japan*
[4]*National Synchrotron Radiation Research Center, 101 Hsin-Ann Road, 30076 Hsinchu, Taiwan*
[5]*Department of Physics, Harvard University, Cambridge, Massachusetts 02138, USA*
[6]*Platform for the Accelerated Realization, Analysis and Discovery of Interface Materials (PARADIM), Cornell University, Ithaca, New York 14853, USA*
[7]*School of Electrical and Computer Engineering, University of Oklahoma, Norman, Oklahoma 73019, USA*
[8]*Center for Quantum Research and Technology, University of Oklahoma, Norman, Oklahoma 73019, USA*
[9]*John A. Paulson School of Engineering and Applied Sciences, Harvard University, Cambridge, Massachusetts 02138, USA*

(Received 24 November 2024; revised 13 March 2025; accepted 17 March 2025; published 1 April 2025)

We examine the bulk electronic structure of $Nd_3Ni_2O_7$ using Ni $2p$ core-level hard x-ray photoemission spectroscopy combined with density functional theory + dynamical mean-field theory. Our results reveal a large deviation of the Ni $3d$ occupation from the formal $Ni^{2.5+}$ valency, highlighting the importance of the charge transfer from oxygen ligands. We find that the dominant d^8 configuration is accompanied by nearly equal contributions from d^7 and d^9 states, exhibiting an unusual valence state among Ni-based oxides. Finally, we discuss the Ni $d_{x^2-y^2}$ and d_{z^2} orbital-dependent hybridization, correlation and local spin dynamics.

DOI: 10.1103/PhysRevB.111.165101

I. INTRODUCTION

Nickel-based complex oxides—nickelates—have drawn considerable attention due to their rich phase diagrams of strongly correlated behavior including metal-to-insulator transitions [1–5], density waves [6–8], magnetism [9–11], and superconductivity [12–16]. The Ruddlesden-Popper nickelates $R_{n+1}Ni_nO_{3n+1}$ in particular also provide a platform for exploring the interplay between structural distortions, electronic correlations, and charge-transfer physics [17,18]. The recent discoveries of superconductivity in the bi- and trilayer compounds ($n = 2, 3$) [14–16,19] have reinvigorated efforts to understand their electronic structure while introducing a new fundamental challenge: the valency of Ni.

In square-planar nickelates, such as prototypical $NdNiO_2$, the low formal valency of Ni^{1+} accommodates self-doping of holes from the rare-earth $5d$ states to the Ni ions, introducing additional complexities in low-energy excitations that are absent in high-T_c cuprates superconductors [20–23]. The bilayer Ruddlesden-Popper $R_3Ni_2O_7$, by comparison, has a formal valency of $Ni^{2.5+}$. The higher Ni valency, i.e., lower Ni $3d$ levels, avoids self-doping from the rare-earth while a stronger charge transfer from the O $2p$ bands may be present [24,25], as is often observed in $RNiO_3$ with a formal Ni^{3+} valency [4,26,27]. Furthermore, the noninteger $Ni^{2.5+}$ valency poses a fundamental question in modeling the electronic structure, particularly regarding the appropriate starting point for the Ni valency and whether it aligns more closely with Ni^{2+} (d^8) or Ni^{3+} (d^7). It is worth stressing that these two electronic configurations exhibit different atomic multiplet structures and effective hybridization with ligands when forming covalent bonds. Thus, this detail represents a fundamental issue that underpins various open questions, including, for example, the importance of multiorbital physics, the origin of the strong orbital dependence in the mass renormalization, and the absence of a static charge order or disproportionation in the quest to understand superconductivity in the bilayer compounds.

One of the most well-established tools for investigating the electronic states of such complex transition metal systems is core-level photoemission spectroscopy (PES) [28,29]. The Ni $2p$ core-level PES measures the dynamical charge response of low-lying valence electrons to the sudden creation of a highly localized core hole at the excited Ni ion, leading to distinct peaks in the spectrum caused by the charge-transfer (CT) from O $2p$ and Ni metallic electrons. These are traditionally referred to as local and nonlocal screening, respectively. By analyzing these peaks, we determine the CT energy parameter

*Contact author: Berit.Goodge@cpfs.mpg.de
†Contact author: hariki@omu.ac.jp

that governs valency and effective hybridization with oxygens in CT-type Ni oxides [30,31]. Core-level PES is particularly suited for such studies due to its high sensitivity to CT effects, unlike charge-neutral methods such as x-ray absorption spectroscopy [29]. This approach, complementary to the low-energy studies about the details at the Fermi level, moves beyond limitations of formal electron counting to extract critical information on Ni $3d$ configuration, correlation effects, and orbital hybridization.

Here, we address this key question by performing core-level hard x-ray photoemission spectroscopy (HAXPES) experiments combined with local density approximation (LDA) + dynamical mean-field theory (DMFT) simulations. By making use of the higher probing depth provided by HAXPES, we are able to study the bulk electronic structure of the bilayer nickelates. Measuring the intrinsic Ni $2p$ core-level spectrum in $La_3Ni_2O_7$, however, is impossible due to severe overlap between the Ni $2p_{3/2}$ and La $3d$ core levels [32–34], as shown in Fig. S3 and discussed more in detail in the Supplemental Material (SM) [35] (see also Refs. [36–40] therein). This overlap has led to conflicting interpretations of the Ni charge state in previous experimental studies [34,41], preventing the extraction of a reliable spectrum for theoretical modeling of the $R_3Ni_2O_7$ system. To overcome this issue, we synthesized $Nd_3Ni_2O_7$ thin films [42,43] which enable direct access to the intrinsic Ni $2p$ spectrum as input for theoretical modeling using the LDA+DMFT method. We show that the system presents a dominant d^8 configuration, with nearly equal contributions from d^7 and d^9, differing from typical Ni^{3+} and Ni^{2+} oxides and requiring all configurations to be considered in theoretical models. We furthermore explore the distinct hybridization and correlation behaviors in the Ni $d_{x^2-y^2}$ and d_{z^2} orbitals, highlighting the orbital-dependent nature of the electronic structure.

II. METHODS

A ~30 nm thin film of $Nd_3Ni_2O_7$ was grown by ozone-assisted molecular-beam epitaxy (MBE) on a stabilizing $LaAlO_3$ substrate, similarly to previous descriptions [42,43] [44]. Comparison of the nominal in-plane bulk and substrate lattice constants indicates a resulting compressive strain of $\varepsilon = (a_{\text{bulk}} - a_{\text{substrate}})/a_{\text{substrate}} \approx -0.9\%$ [42,43], smaller than that reported in thin films of $La_3Ni_2O_7$ which exhibit superconductivity [16,19]. Annular dark-field scanning transmission electron microscopy (ADF-STEM) investigation of the film structure shows good adherence to the bilayer Ruddlesden-Popper structure [35]. HAXPES measurements were performed at the Max-Planck-NSRRC HAXPES end station with the MB Scientific A-1 HE analyzer, Taiwan undulator beamline BL12XU of SPring-8 [45]. Photon energies of $h\nu = 6.5$ keV and 10 keV with resolutions of around 270 meV and 320 meV, respectively, were used. Soft x-ray photoelectron spectroscopy experiments were performed at the NSRRC-MPI TPS 45A submicron soft x-ray spectroscopy beamline at the Taiwan Photon Source in Taiwan [46]. The photon energy was set to 1.2 keV, with a resolution of around 150 meV. All measurements were performed at 80 K.

LDA+DMFT calculations were performed with the implementation in Refs. [30,31,47] for a lattice model spanning

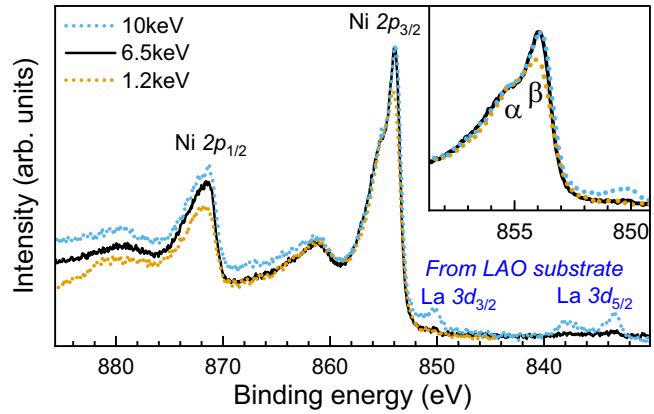

FIG. 1. Ni $2p$ core level spectra measured with photon energies of 10 keV (blue dotted line), 6.5 keV (black line), and 1.2 keV (orange dotted line).

Ni $3d$ and O $2p$ bands derived from the LDA calculations [48–50]. Based on previous DMFT studies for $La_3Ni_2O_7$ [51–53], we used Hubbard U and Hund's J values of (6.0 eV, 0.95 eV) within the Ni $3d$ shell. These values give the configuration-averaged Coulomb interaction of $U_{dd} = U - 4/9J = 5.57$ eV [31]. After obtaining a converged DMFT solution with the continuous-time quantum Monte Carlo solver for the Anderson impurity model (AIM), we calculated valence-band spectra and hybridization densities $\Delta(\varepsilon)$ on the real frequency axis, followed by analytical continuation of the self-energy using the maximum entropy method [54]. Finally, we computed the Ni $2p$ core-level PES spectrum from the AIM, incorporating $\Delta(\varepsilon)$ and $2p$ core orbitals [30,31]. Computational details and the robustness of our results with the model parameters are provided in the SM [35] (see also Refs. [55–57] therein).

In LDA+X methods, a double-counting correction μ_{dc} needs to be introduced to account for dd interaction effects present in the LDA results. Though a universally accepted form for μ_{dc} is unavailable [58–60], it controls Ni $3d$ levels relative to O $2p$ bands, thus the CT energy. Following Ref. [30], we use the linear function $\Delta_{dp} = (\varepsilon_d - \mu_{\text{dc}}) + 7.5 \times U_{\text{dd}} - \varepsilon_p$, mimicking the CT energy in a cluster model analysis. Here, ε_d and ε_p refer to the LDA orbital energies of Ni $3d$ and O $2p$, and U_{dd} is the averaged d–d interaction. Realistic Δ_{dp} values are obtained by comparing simulated Ni $2p$ core-level results to the experimental HAXPES spectrum.

III. RESULTS

Figure 1 shows the Ni $2p$ core-level photoemission spectra obtained using 10, 6.5, and 1.2 keV photons. Overall, the Ni $2p$ core level displays a set of structures commonly seen in other nickelates [34,61,62]. The main Ni $2p_{3/2}$ peak shows two distinct features corresponding to the local (α) and nonlocal metallic (β) screening processes, and a CT satellite at around 861.5 eV. Around 17 eV above the Ni $2p_{3/2}$, we observe a similar structure for the Ni $2p_{1/2}$, albeit broader due to the shorter core-hole lifetime. Depending on the photon energy, we observe some differences in the spectra. In the 10 keV data, there is a weak double peak at 833 and

838 eV, as well as one peak at 850 eV next to the Ni $2p_{3/2}$, matching the double peak structures of La $3d$ commonly seen in La-containing perovskite oxides [38], with the La $3d_{3/2}$ partially overlapping with the Ni $2p_{3/2}$ [34]. These peaks are contributions from the $LaAlO_3$ substrate below the $Nd_3Ni_2O_7$, which appear when using high photon energies with larger probing depth [63]. Indeed, at 6.5 keV, the La $3d$ features are reduced almost completely despite the relative increase of the La $3d$ cross sections compared to those of Ni $2p$ [64], indicating that the probing depth using 6.5 keV is barely enough to reach the substrate. This thus confirms the bulk sensitivity of the measurements and that the collected Ni $2p$ spectra are well representative of the whole $Nd_3Ni_2O_7$ film depth, as evidenced by good agreement in the Ni $2p$ derived features for 10 keV and 6.5 keV despite their different probing depths.

The surface-sensitive 1.2 keV spectrum, on the other hand, shows noticeable differences compared to the higher probing energy data. The electronic structure at the vicinity of the surface is thus clearly distinct from that of the bulk, with the significant reduction of the peak β indicating a suppression of the nonlocal metallic screening at the surface layers. Differences between the bulk and surface electronic structure are often known to occur in strongly correlated transition metal oxides [65–71], with phenomena like polar surfaces, relaxation, or reconstructions in the surface, etc., leading to significantly different properties and band structure near the surface, thus making bulk sensitivity crucial to ensure that the experimental results are intrinsic and representative of the bulk of the material. It is important to note the observation of these differences at 1.2 keV, i.e., Ni $2p$ core level photoelectrons with 300–350 eV kinetic energy, which are expected to have higher probing depths than common vacuum ultraviolet (VUV) valence band ARPES experiments.

Having established that the 6.5 keV HAXPES measurements best represent the bulk $Nd_3Ni_2O_7$ thin film, we use these measurements to determine the Δ_{dp} parameter by comparison to LDA+DMFT calculations. In Figs. 2(a) and 2(b), the Ni $2p_{3/2}$ spectra are computed for selected Δ_{dp} values. With increasing Δ_{dp}, the ligand levels shift deeper relative to the Fermi level, leading to a larger energy splitting between the local screening α (mainly from nearest-neighboring oxygens) and the nonlocal metallic screening β features. In the close-up shown in Fig. 2(b), we observe that the experimental splitting and $\alpha - \beta$ ratio is best reproduced by $\Delta_{dp} = 3.5$ eV, with 4.5 eV also yielding a reasonable agreement. Next, we observe in Fig. 2(a) that the weight ratio between the main peak and the satellite is also highly sensitive to the Δ_{dp} value, with the satellite spectral weight decreasing with increasing Δ_{dp}. Here, the best agreement is obtained between $\Delta_{dp} = 3.5$ eV and 2.5 eV. These two observations allow us to constrain its realistic value of around $\Delta_{dp} = 3.5$ eV. In the SM [35], we computed the Ni $2p$ spectrum for not only different values of Δ_{dp} but also for different values of U. We found that the experimental spectrum is best reproduced by the chosen U, although the sensitivity to the precise value of U is not very large.

The Δ_{dp}, which measures energy splitting of the Ni $3d$ and O $2p$ levels, is a key parameter for the d-electron charge states in CT-type systems according to the Zaanen-Sawatzky-Allen

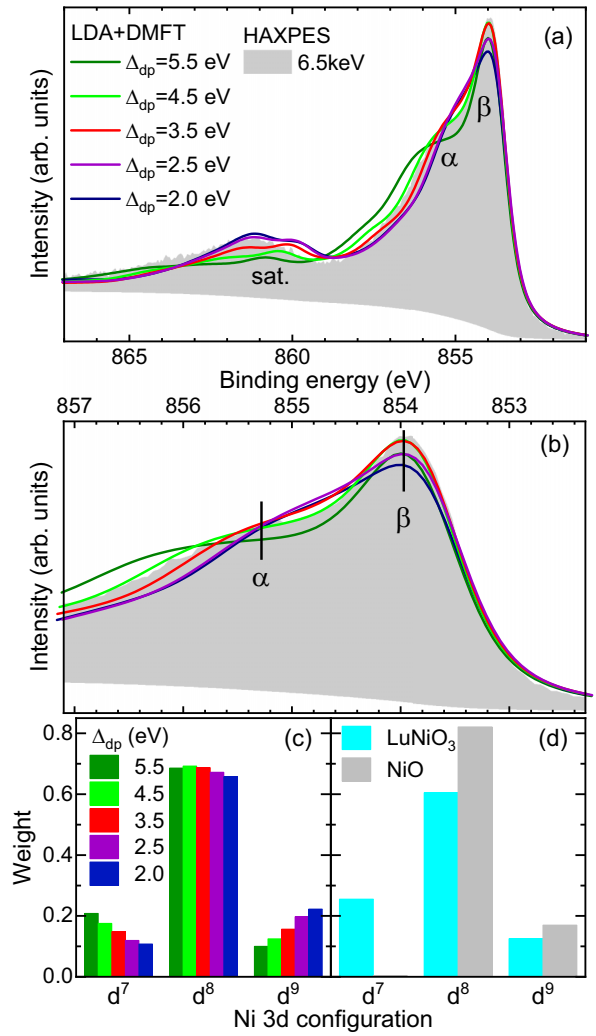

FIG. 2. (a) LDA+DMFT fit together with the experimental Ni $2p_{3/2}$ HAXPES spectrum. (b) Close-up of the Ni $2p_{3/2}$ α and β features. (c) Atomic configuration histogram of the Ni $3d$ states in $Nd_3Ni_2O_7$, computed with the selected Δ_{dp} values. (d) Atomic configuration histograms for reference Ni oxides: metallic $LuNiO_3$ (cyan) [72] and NiO (gray) [35].

(ZSA) diagram [73]. In Fig. 2(c), the Ni $3d$ charge state is quantified by computing an atomic histogram at the Ni site in DMFT solutions for various Δ_{dp} values. Regardless of Δ_{dp}, the d^8 configuration exhibits a dominant peak in the histogram, with a large distribution toward the d^7 and d^9 configurations which depend on the Δ_{dp} value: a smaller Δ_{dp} increases the d^9 weight, and vice versa. At the optimal value determined above, the d^7 and d^9 weights are nearly identical. As shown in Fig. S6 of the SM [35], the d-configuration distribution in the atomic histogram is predominantly determined by Δ_{dp}, with negligible influence from the Coulomb interaction U, as expected for a system in the CT-type regime of the ZSA diagram.

The charge state contrasts with that of divalent or trivalent Ni oxides. In Fig. 2(d), the histograms for NiO and metallic $LuNiO_3$, which are prototype systems of formally Ni^{2+} and Ni^{3+} oxides, respectively, are shown. The reference data are taken from Ref. [72,74] and an additional DMFT simulation

based on Ref. [47]. NiO exhibits a predominant d^8 peak with a distribution toward the d^9 state. In the high-valency $LuNiO_3$, with deeper Ni $3d$ levels, the CT energy is, as in other formally Ni^{3+} oxides [4,75,76], small or even negative, facilitating CT from O $2p$ states and resulting in a dominant d^8 state. The larger weight of the d^7 state compared to that of d^9 reflects its high formal valency. For an optimal Δ_{dp} of 3.5 eV, the charge state of $Nd_3Ni_2O_7$, with formally $Ni^{+2.5}$, is qualitatively different from these reference Ni oxides, and all the d^7–d^9 electronic configurations need to be considered when modeling its electronic structure. The mean Ni occupation of nearly d^8, deviating from the expected $d^{\sim 7.5}$ for a formal $Ni^{+2.5}$ valency, suggests that charge-transfer from O $2p$ states is significant in $Nd_3Ni_2O_7$. Note as Δ_{dp} is reduced (increased), the d configuration shifts to more closely resemble either divalent (trivalent) case. The d occupation in $LuNiO_3$ [72] is 7.84, exhibiting a larger deviation from its formal valency than that in $Nd_3Ni_2O_7$, which is consistent with Δ_{dp} of 3.5 eV in $Nd_3Ni_2O_7$ being moderate.

IV. DISCUSSION

Our results are consistent with the recent study [34] which indicated the absence of charge disproportionation (CD) signatures in $La_3Ni_2O_7$. Our LDA+DMFT calculations do not indicate any instability toward a CD [77]. Its absence would be unsurprising, given that the Ni d charge states [Figs. 2(b) and 2(c)] as well as the crystal structure of $R_3Ni_2O_7$ differ from those of $RNiO_3$, where CD is widely observed. The standard picture of CD in $RNiO_3$ depends on a delicate balance between the three-dimensional tilting pattern of NiO_6 octahedra and the correlated Ni $3d$ charge states [1,78–82], while the bilayer Ruddlesden-Popper compounds should host distinct octahedral distortions due to their reduced structural dimensionality. Theoretical models suggest these distortions are likely tied to the emergence of superconductivity under suitable pressure conditions [83], particularly in relation to orbital anisotropy, which we return to below.

The clarification of the Ni d state has implications for understanding low-energy excitations. Although the Ni d^8 valence configuration weight remains almost unchanged over a wide range of Δ_{dp}, as shown in Fig. 2(c), this does not necessarily imply that low-energy excitations are unaffected. In Fig. 3(a), the quasiparticle mass enhancement m^*/m of the Ni $d_{x^2-y^2}$ and d_{z^2} states was calculated from the converged DMFT self-energies $\Sigma(i\omega_n)$, as $m^*/m = Z^{-1} = [1 - \partial \mathrm{Im}\Sigma(i\omega)/\partial\omega]_{\omega\to 0^+}$, where the m is noninteracting band mass and Z is the renormalization factor. In addition to strong orbital dependence, the m^*/m of the two orbitals exhibits a pronounced dependence on the Δ_{dp} value, as the O $2p$ states are present near the Fermi energy E_F in this CT-type oxide and thus directly influence the degree of the localization of the Ni $3d$ electrons, see the SM [35] for the Δ_{dp} dependence of the DMFT valence-band spectra. A recent ARPES study on $La_3Ni_2O_7$ estimated m^*/m to be in the range of 1–3 for the $d_{x^2-y^2}$ state and 5–8 for the d_{z^2} state by rescaling DFT and DFT+U bands to match ARPES results in part of the Brillouin zone [84]. The calculated m^*/m values for the Δ_{dp} range that reproduces the Ni $2p$ data in Fig. 2, highlighted in gray in Fig. 3(a), are comparable to the reported values.

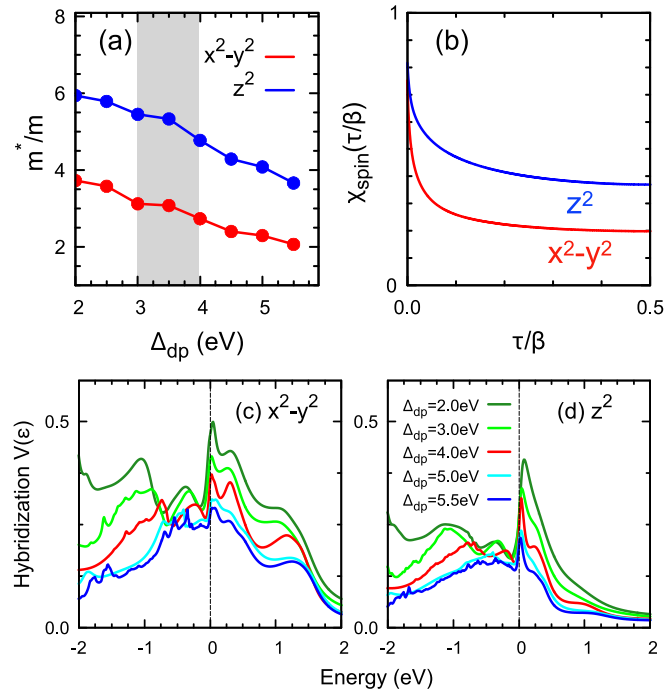

FIG. 3. (a) The mass enhancement m^*/m of the Ni $d_{x^2-y^2}$ and d_{z^2} states as a function of the Δ_{dp} parameters. The region in gray shadow indicates the realistic values estimated by the Ni $2p$ XPS analysis in Fig. 2. (b) The orbital-diagonal component of the local spin correlation function $\chi_{\mathrm{spin}}(\tau)$ with $\Delta_{dp} = 3.5$ eV, where τ represents the imaginary time. The Ni hybridization densities $V_\gamma(\omega)$ for (c) the $d_{x^2-y^2}$ state and (d) the d_{z^2} state, calculated with the different Δ_{dp} values. All results in the panels are calculated using the LDA+DMFT method at $T = 300$ K.

Orbital dependence has been at the center of discussions in the bilayer nickelates [51,84–88]. To gain an insight into it, in Figs. 3(c) and 3(d), we compare the Ni hybridization densities $V_\gamma(\omega)$ ($\gamma = x^2 - y^2, z^2$), which represent the exchange amplitude of an electron between the local d_γ state and lattice. The sharp evolution near E_F in $V_\gamma(\omega)$ as a function of Δ_{dp} accounts for the sensitivity of the metallic screening feature β in Ni $2p$ core-level PES to the Δ_{dp} values in Fig. 2(a). Overall, the Ni $d_{x^2-y^2}$ state exhibits stronger hybridization with the low-energy states compared to the Ni d_{z^2} state, which is likely responsible for the weaker m^*/m for the former orbital than the latter one. This observation is consistent with the orbital-dependent spin screening encoded in the time-dependent local spin correlation function $\chi_{\mathrm{spin}}(\tau)$, calculated for the LDA+DMFT result with the optimal Δ_{dp} in Fig. 3(b). $\chi_{\mathrm{spin}}(\tau)$ characterizes the dynamics of the local spin, influenced by hybridization with the crystal and many-body correlations [39,89,90]. We find a finite and nearly identical response at $\tau = 0^+$ for both orbitals, indicating that an instantaneous spin of approximately $S = 1/2$ is present in each. However, the Ni $d_{x^2-y^2}$ electron undergoes faster spin screening than the d_{z^2} orbital over time, reflecting the orbital-dependent hybridization. In the Appendix, we demonstrate through additional LDA+DMFT AIM calculations that the orbital-dependent hybridization near E_F is also important for

the formation of the β feature observed in the experimental Ni $2p$ core-level spectrum in Fig. 2(a).

The m^*/m values obtained for the ambient pressure phase in this study differ from those calculated for the high-pressure phase in several theoretical studies of $La_3Ni_2O_7$ [51,87], e.g., $m^*/m \sim 3$ and 2.3 for the $d_{x^2-y^2}$ and d_{z^2} states, respectively, in Ref. [51]. As expected, m^*/m is reduced in the high-pressure phase due to the increased bandwidth of the Ni $3d$ states compared to the ambient pressure, while the orbital-dependent localization behavior persists in the high pressure phase. In the future, extending the approach described here to epitaxially strained thin films could provide further insight to the evolution of such parameters with structural tuning.

V. CONCLUSIONS

In summary, we have characterized the bulk electronic structure of a bilayer nickelate $Nd_3Ni_2O_7$ thin film using Ni $2p$ core-level hard x-ray photoemission spectroscopy (HAXPES) combined with LDA+DMFT simulations. Comparison of the surface-sensitive PES and bulk-sensitive HAXPES measurements show significant differences between the surface and bulk electronic structures in this compound. We experimentally observed both local and nonlocal screening features in the Ni $2p_{3/2}$ core-level spectrum, which was not feasible in La-based samples studied so far due to overlapping La $3d$ and Ni $2p$ core levels. Guided by the observed core-level features, we performed parameter optimization in the LDA+DMFT calculations and determined the charge-transfer energy, a key parameter for the Ni valency and the hybridization with the oxygen ligands in this charge-transfer-type system. Our results show a dominant d^8 (Ni^{2+}) configuration ($\sim$70%), with nearly equal contributions from d^7 (Ni^{3+}) and d^9 (Ni^{1+}) ones. This charge distribution differs from typical Ni^{3+} oxides like $RNiO_3$ and Ni^{2+} oxides like NiO, requiring all configurations to be considered in theoretical models. Moreover, the Ni $d_{x^2-y^2}$ orbital exhibited stronger hybridization compared to the d_{z^2} orbital, leading to distinct correlation (mass renormalization) and spin dynamic behaviors in the two orbitals. This highlights the orbital-dependent nature of the electronic structure and correlations in this system.

ACKNOWLEDGMENTS

We thank M. Kitatani for valuable discussions. D.T. acknowledges the support by the Deutsche Forschungsgemeinschaft (DFG, German Research Foundation) under the Walter Benjamin Programme, Projektnummer 521584902. A.H. was supported by JSPS KAKENHI Grants No. 21K13884, No. 23K03324, and No. 23H03817. B.H.G. was supported by Schmidt Science Fellows in partnership with the Rhodes Trust. We acknowledge the support for the measurements from the Max Planck-POSTECH-Hsinchu Center for Complex Phase Materials. G.A.P. and D.F.S. are primarily supported by the U.S. Department of Energy (DOE), Office of Basic Energy Sciences, Division of Materials Sciences and Engineering, under Award No. DE SC0021925; and by NSF Graduate Research Fellowship Grant No. DGE-1745303. G.A.P. acknowledges additional support from the Paul and Daisy Soros Fellowship for New Americans. Q.S. was supported by the Science and Technology Center for Integrated Quantum Materials, NSF Grant No. DMR-1231319. J.A.M. acknowledges support from the U.S. Department of Energy (DOE), Office of Basic Energy Sciences, Division of Materials Sciences and Engineering, under Award No. DE SC0021925. Materials growth was supported by PARADIM under National Science Foundation (NSF) Cooperative Agreement No. DMR-2039380. The computation in this work has been done using the facilities of the Supercomputer Center, the Institute for Solid State Physics, the University of Tokyo.

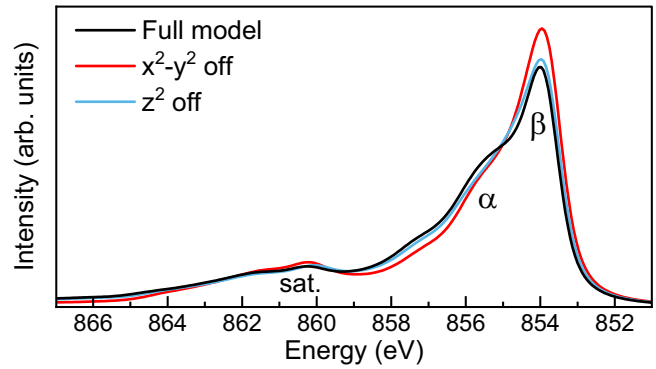

FIG. 4. Ni $2p$ core-level PES spectra calculated using the LDA+DMFT AIM method for the full (black) and modified models with no hybridization of the $d_{x^2-y^2}$ orbital (red) and the d_{z^2} orbital (blue) with metallic states near E_F. See text for detailed explanations of models.

APPENDIX: ORBITAL DEPENDENT HYBRIDIZATION EFFECT IN Ni $2p$ SPECTRUM

In Fig. 4, we calculate the PES spectra using the LDA+DMFT AIM with modified $V_\gamma(\omega)$, where the hybridization densities within the [−1.0 eV, 1.0 eV] window in Figs. 3(c) and 3(d) are manually set to zero when simulating the PES final states, meaning that CT screening from the metallic states near E_F does not appear in the simulated spectra. The spectra exhibit intensity modulations of the metallic screening feature β, with the large suppression of β being more closely related to the hybridization of the Ni $d_{x^2-y^2}$ state rather than the d_{z^2} state. This additional piece of evidence derived from the Ni $2p$ core-level PES spectra further confirms that there is an orbital-dependent hybridization, with the Ni $d_{x^2-y^2}$ state exhibiting a stronger hybridization with the low-energy states compared to the Ni d_{z^2}.

[1] A. Mercy, J. Bieder, J. Íñiguez, and P. Ghosez, Structurally triggered metal-insulator transition in rare-earth nickelates, Nat. Commun. **8**, 1677 (2017).

[2] V. Pardo and W. E. Pickett, Metal-insulator transition in layered nickelates $La_3Ni_2O_{7-\delta}$ ($\delta = 0.0, 0.5, 1$), Phys. Rev. B **83**, 245128 (2011).

[3] R Jaramillo, S. D. Ha, D. M. Silevitch, and S. Ramanathan, Origins of bad-metal conductivity and the insulator–metal transition in the rare-earth nickelates, Nat. Phys. **10**, 304 (2014).

[4] V. Bisogni, S. Catalano, R. J. Green, M. Gibert, R. Scherwitzl, Y. Huang, V. N. Strocov, P. Zubko, S. Balandeh, J.-M. Triscone, G. Sawatzky, and T. Schmitt, Ground-state oxygen holes and the metal–insulator transition in the negative charge-transfer rare-earth nickelates, Nat. Commun. **7**, 13017 (2016).

[5] S. Johnston, A. Mukherjee, I. Elfimov, M. Berciu, and G. A. Sawatzky, Charge disproportionation without charge transfer in the rare-earth-element nickelates as a possible mechanism for the metal-insulator transition, Phys. Rev. Lett. **112**, 106404 (2014).

[6] C. C. Tam, J. Choi, X. Ding, S. Agrestini, A. Nag, M. Wu, B. Huang, H. Luo, P. Gao, M. García-Fernández *et al.*, Charge density waves in infinite-layer $NdNiO_2$ nickelates, Nat. Mater. **21**, 1116 (2022).

[7] J. Zhang, D. Phelan, A. S. Botana, Y.-S. Chen, H. Zheng, M. Krogstad, S. G. Wang, Y. Qiu, J. A. Rodriguez-Rivera, R. Osborn *et al.*, Intertwined density waves in a metallic nickelate, Nat. Commun. **11**, 6003 (2020).

[8] K. Chen, X. Liu, J. Jiao, M. Zou, C. Jiang, X. Li, Y. Luo, Q. Wu, N. Zhang, Y. Guo *et al.*, Evidence of spin density waves in $La_3Ni_2O_{7-\delta}$, Phys. Rev. Lett. **132**, 256503 (2024).

[9] J. Fowlie, M. Hadjimichael, M. M. Martins, D. Li, M. Osada, B. Y. Wang, K. Lee, Y. Lee, Z. Salman, T. Prokscha *et al.*, Intrinsic magnetism in superconducting infinite-layer nickelates, Nat. Phys. **18**, 1043 (2022).

[10] H. Lu, M. Rossi, A. Nag, M. Osada, D. F. Li, K. Lee, B. Y. Wang, M. Garcia-Fernandez, S. Agrestini, Z. X. Shen *et al.*, Magnetic excitations in infinite-layer nickelates, Science **373**, 213 (2021).

[11] R. A. Ortiz, P. Puphal, M. Klett, F. Hotz, R. K. Kremer, H. Trepka, M. Hemmida, H.-A. K. von Nidda, M. Isobe, R. Khasanov, H. Luetkens, P. Hansmann, B. Keimer, T. Schafer, and M. Hepting, Magnetic correlations in infinite-layer nickelates: An experimental and theoretical multimethod study, Phys. Rev. Res. **4**, 023093 (2022).

[12] D. Li, K. Lee, B. Y. Wang, M. Osada, S. Crossley, H. R. Lee, Y. Cui, Y. Hikita, and H. Y. Hwang, Superconductivity in an infinite-layer nickelate, Nature (London) **572**, 624 (2019).

[13] G. A. Pan, D. Ferenc Segedin, H. LaBollita, Q. Song, E. M. Nica, B. H. Goodge, A. T. Pierce, S. Doyle, S. Novakov, D. Córdova Carrizales, A. T. N'Diaye, P. Shafer, H. Paik, J. T. Heron, J. A. Mason, A. Yacoby, L. F. Kourkoutis, O. Erten, C. M. Brooks, A. S. Botana, and J. A. Mundy, Superconductivity in a quintuple-layer square-planar nickelate, Nat. Mater. **21**, 160 (2022).

[14] H. Sun, M. Huo, X. Hu, J. Li, Z. Liu, Y. Han, L. Tang, Z. Mao, P. Yang, B. Wang, J. Cheng, D.-X. Yao, G.-M. Zhang, and M. Wang, Signatures of superconductivity near 80 k in a nickelate under high pressure, Nature (London) **621**, 493 (2023).

[15] Y. Zhu, D. Peng, E. Zhang, B. Pan, X. Chen, L. Chen, H. Ren, F. Liu, Y. Hao, N. Li *et al.*, Superconductivity in pressurized trilayer $La_4Ni_3O_{10-\delta}$ single crystals, Nature (London) **631**, 531 (2024).

[16] E. K. Ko, Y. Yu, Y. Liu, L. Bhatt, J. Li, V. Thampy, C.-T. Kuo, B. Y. Wang, Y. Lee, K. Lee, J.-S. Lee, B. H. Goodge, D. A. Muller, and H. Y. Hwang, Signatures of ambient pressure superconductivity in thin film $La_3Ni_2O_7$, Nature (London) **638**, 935 (2025).

[17] T. Cui, S. Choi, T. Lin, C. Liu, G. Wang, N. Wang, S. Chen, H. Hong, D. Rong, Q. Wang *et al.*, Strain-mediated phase crossover in Ruddlesden–Popper nickelates, Commun. Mater. **5**, 32 (2024).

[18] W. Sun, Y. Li, X. Cai, J. Yang, W. Guo, Z. Gu, Y. Zhu, and Y. Nie, Electronic and transport properties in Ruddlesden-Popper neodymium nickelates $Nd_{n+1}Ni_nO_{3n+1}$(n=1-5), Phys. Rev. B **104**, 184518 (2021).

[19] G. Zhou, W. Lv, H. Wang, Z. Nie, Y. Chen, Y. Li, H. Huang, W. Chen, Y. Sun, Q.-K. Xue *et al.*, Ambient-pressure superconductivity onset above 40 k in bilayer nickelate ultrathin films, arXiv:2412.16622.

[20] B. Y. Wang, K. Lee, and B. H. Goodge, Experimental progress in superconducting nickelates, Annu. Rev. Condens. Matter Phys. **15**, 305 (2024).

[21] H. Sakakibara, H. Usui, K. Suzuki, T. Kotani, H. Aoki, and K. Kuroki, Model construction and a possibility of cupratelike pairing in a new d^9 nickelate superconductor (Nd, Sr)NiO_2, Phys. Rev. Lett. **125**, 077003 (2020).

[22] M. Kitatani, L. Si, O. Janson, R. Arita, Z. Zhong, and K. Held, Nickelate superconductors—a renaissance of the one-band Hubbard model, npj Quantum Mater. **5**, 59 (2020).

[23] M. Hirayama, T. Tadano, Y. Nomura, and R. Arita, Materials design of dynamically stable d^9 layered nickelates, Phys. Rev. B **101**, 075107 (2020).

[24] Z. Dong, M. Huo, J. Li, J. Li, P. Li, H. Sun, L. Gu, Y. Lu, M. Wang, Y. Wang, and Z. Chen, Visualization of oxygen vacancies and self-doped ligand holes in $La_3Ni_2O_{7-\delta}$, Nature (London) **630**, 847 (2024).

[25] X. Chen, J. Choi, Z. Jiang, J. Mei, K. Jiang, J. Li, S. Agrestini, M. Garcia-Fernandez, H. Sun, X. Huang, D. Shen, M. Wang, J. Hu, Y. Lu, K.-J. Zhou, and D. Feng, Electronic and magnetic excitations in $La_3Ni_2O_7$, Nat. Commun. **15**, 9597 (2024).

[26] S. Catalano, M. Gibert, J. Fowlie, J. Íñiguez, J. M. Triscone, and J. Kreisel, Rare-earth nickelates $RNiO_3$: thin films and heterostructures, Rep. Prog. Phys. **81**, 046501 (2018).

[27] R. J. Green, M. W. Haverkort, and G. A. Sawatzky, Bond disproportionation and dynamical charge fluctuations in the perovskite rare-earth nickelates, Phys. Rev. B **94**, 195127 (2016).

[28] S. Hüfner, *Photoelectron Spectroscopy* (Advanced Texts in Physics, Springer, Berlin, Heidelberg, 2003).

[29] F. de Groot and A. Kotani, *Core Level Spectroscopy of Solids* (CRC Press, Boca Raton, 2008).

[30] K. Higashi, M. Winder, J. Kuneš, and A. Hariki, Core-level x-ray spectroscopy of infinite-layer nickelate: LDA + DMFT study, Phys. Rev. X **11**, 041009 (2021).

[31] A. Hariki, T. Uozumi, and J. Kuneš, LDA+DMFT approach to core-level spectroscopy: Application to 3*d* transition metal compounds, Phys. Rev. B **96**, 045111 (2017).

[32] S. Mickevičius, S. Grebinskij, V. Bondarenka, B. Vengalis, K. Šliužienė, B. A. Orlowski, V. Osinniy, and W. Drube, Investigation of epitaxial $LaNiO_{3-x}$ thin films by high-energy XPS, J. Alloys Compd. **423**, 107 (2006).

[33] K. Yamagami, K. Ikeda, A. Hariki, Y. Zhang, A. Yasui, Y. Takagi, Y. Hotta, T. Katase, T. Kamiya, and H. Wadati, Hard x-ray photoemission study on strain effect in $LaNiO_3$ thin films, Appl. Phys. Lett. **118**, 161601 (2021).

[34] D. Takegami, K. Fujinuma, R. Nakamura, M. Yoshimura, K.-D. Tsuei, G. Wang, N. N. Wang, J.-G. Cheng, Y. Uwatoko, and T. Mizokawa, Absence of Ni^{2+}/Ni^{3+} charge disproportionation and possible roles of O $2p$ holes in $La_3Ni_2O_{7-\delta}$ revealed by hard x-ray photoemission spectroscopy, Phys. Rev. B **109**, 125119 (2024).

[35] See Supplemental Material at http://link.aps.org/supplemental/10.1103/PhysRevB.111.165101 for additional experimental data as well as complementary calculations.

[36] A. Kotani and H. Ogasawara, Theory of core-level spectroscopy of rare-earth oxides, J. Electron Spectrosc. Relat. Phenom. **60**, 257 (1992).

[37] H. Eisaki, S. Uchida, T. Mizokawa, H. Namatame, A. Fujimori, J. van Elp, P. Kuiper, G. A. Sawatzky, S. Hosoya, and H. Katayama-Yoshida, Electronic structure of $La_{2-x}Sr_xNiO_4$ studied by photoemission and inverse-photoemission spectroscopy, Phys. Rev. B **45**, 12513 (1992).

[38] D. J. Lam, B. W. Veal, and D. E. Ellis, Electronic structure of lanthanum perovskites with 3*d* transition elements, Phys. Rev. B **22**, 5730 (1980).

[39] D. Takegami, C.-Y. Kuo, K. Kasebayashi, J.-G. Kim, C. F. Chang, C. E. Liu, C. N. Wu, D. Kasinathan, S. G. Altendorf, K. Hoefer, F. Meneghin, A. Marino, Y. F. Liao, K. D. Tsuei, C. T. Chen, K.-T. Ko, A. Günther, S. G. Ebbinghaus, J. W. Seo, D. H. Lee, G. Ryu, A. C. Komarek, S. Sugano, Y. Shimakawa, A. Tanaka, T. Mizokawa, J. Kuneš, L. H. Tjeng, and A. Hariki, $CaCu_3Ru_4O_{12}$: A high-Kondo-temperature transition-metal oxide, Phys. Rev. X **12**, 011017 (2022).

[40] D. Takegami, L. Nicolaï, Y. Utsumi, A. Meléndez-Sans, D. A. Balatsky, C.-A. Knight, C. Dalton, S.-L. Huang, C.-S. Chen, L. Zhao, A. C. Komarek, Y.-F. Liao, K.-D. Tsuei, J. Minár, and L. H. Tjeng, Direct imaging of valence orbitals using hard x-ray photoelectron spectroscopy, Phys. Rev. Res. **4**, 033108 (2022).

[41] Z. Liu, H. Sun, M. Huo, X. Ma, Y. Ji, E. Yi, L. Li, H. Liu, J. Yu, Z. Zhang, Z. Chen, F. Liang, H. Dong, H. Guo, D. Zhong, B. Shen, S. Li, and M. Wang, Evidence for charge and spin density waves in single crystals of $La_3Ni_2O_7$ and $La_3Ni_2O_6$, Sci. China Phys. Mech. Astron. **66**, 217411 (2023).

[42] G. A. Pan, Q. Song, D. Ferenc Segedin, M.-C. Jung, H. El-Sherif, E. E. Fleck, B. H. Goodge, S. Doyle, D. Córdova Carrizales, A. T. N'Diaye, P. Shafer, H. Paik, L. F. Kourkoutis, I. ElBaggari, A. S. Botana, C. M. Brooks, and J. A. Mundy, Synthesis and electronic properties of $Nd_{n+1}Ni_nO_{3n+1}$ Ruddlesden-Popper nickelate thin films, Phys. Rev. Mater. **6**, 055003 (2022).

[43] D. Ferenc Segedin, B. H. Goodge, G. A. Pan, Q. Song, H. LaBollita, M.-C. Jung, H. El-Sherif, S. Doyle, A. Turkiewicz, N. K. Taylor *et al.*, Limits to the strain engineering of layered square-planar nickelate thin films, Nat. Commun. **14**, 1468 (2023).

[44] The film was synthesized at a substrate temperature of 670 °C as measured by a thermocouple and under a chamber pressure of 3×10^{-6} Torr distilled ozone. The nickel and neodymium effusion cell temperatures were adjusted to yield a flux of approximately 2×10^{13} atoms/cm^{2}s as measured by a quartz crystal microbalance and subsequently fine tuned using the $NdNiO_3$ calibration procedure detailed in Ref. [42].

[45] D. Takegami, L. Nicolaï, T. C. Koethe, D. Kasinathan, C. Y. Kuo, Y. F. Liao, K. D. Tsuei, G. Panaccione, F. Offi, G. Monaco, N. B. Brookes, J. Minár, and L. H. Tjeng, Valence band hard x-ray photoelectron spectroscopy on 3*d* transition-metal oxides containing rare-earth elements, Phys. Rev. B **99**, 165101 (2019).

[46] H.-M. Tsai, H.-W. Fu, C.-Y. Kuo, L.-J. Huang, C.-S. Lee, C.-Y. Hua, K.-Y. Kao, H.-J. Lin, H.-S. Fung, S.-C. Chung, C.-F. Chang, A. Chainani, L. H. Tjeng, and C.-T. Chen, A submicron soft x-ray active grating monochromator beamline for ultra-high resolution angle-resolved photoemission spectroscopy, AIP Conf. Proc. **2054**, 060047 (2019).

[47] A. Hariki, M. Winder, T. Uozumi, and J. Kuneš, LDA + DMFT approach to resonant inelastic x-ray scattering in correlated materials, Phys. Rev. B **101**, 115130 (2020).

[48] P. Blaha, K. Schwarz, G. Madsen, D. Kvasnicka, and J. Luitz, *WIEN2k, An Augmented Plane Wave + Local Orbitals Program for Calculating Crystal Properties* (Karlheinz Schwarz, Techn. Universitat Wien, Austria, ISBN 3-9501031-1-2, 2001).

[49] J. Kuneš, R. Arita, P. Wissgott, A. Toschi, H. Ikeda, and K. Held, Wien2wannier: From linearized augmented plane waves to maximally localized wannier functions, Comput. Phys. Commun. **181**, 1888 (2010).

[50] A. A. Mostofi, J. R. Yates, G. Pizzi, Y.-S. Lee, I. Souza, D. Vanderbilt, and N. Marzari, An updated version of wannier90: A tool for obtaining maximally-localised wannier functions, Comput. Phys. Commun. **185**, 2309 (2014).

[51] D. A. Shilenko and I. V. Leonov, Correlated electronic structure, orbital-selective behavior, and magnetic correlations in double-layer $La_3Ni_2O_7$ under pressure, Phys. Rev. B **108**, 125105 (2023).

[52] X. Wan, V. Ivanov, G. Resta, I. Leonov, and S. Y. Savrasov, Exchange interactions and sensitivity of the ni two-hole spin state to hund's coupling in doped $NdNiO_2$, Phys. Rev. B **103**, 075123 (2021).

[53] I. Leonov, S. L. Skornyakov, and S. Y. Savrasov, Lifshitz transition and frustration of magnetic moments in infinite-layer $NdNiO_2$ upon hole doping, Phys. Rev. B **101**, 241108(R) (2020).

[54] M. Jarrell and J. E. Gubernatis, Bayesian inference and the analytic continuation of imaginary-time quantum Monte Carlo data, Phys. Rep. **269**, 133 (1996).

[55] V. I. Voronin, I. F. Berger, V. A. Cherepanov, L. Ya. Gavrilova, A. N. Petrov, A. I. Ancharov, B. P. Tolochko, and S. G. Nikitenko, Neutron diffraction, synchrotron radiation and EXAFS spectroscopy study of crystal structure peculiarities of the lanthanum nickelates $La_{n+1}Ni_nO_y$ (n=1,2,3), Nucl. Instrum. Methods Phys. Res., Sect. A **470**, 202 (2001).

[56] M. Ghiasi, A. Hariki, M. Winder, J. Kuneš, A. Regoutz, T.-L. Lee, Y. Hu, J.-P. Rueff, and F. M. F. de Groot, Charge-transfer effect in hard x-ray 1*s* and 2*p* photoemission spectra: LDA + DMFT and cluster-model analysis, Phys. Rev. B **100**, 075146 (2019).

[57] P. Werner, A. Comanac, L. de' Medici, M. Troyer, and A. J. Millis, Continuous-time solver for quantum impurity models, Phys. Rev. Lett. **97**, 076405 (2006).

[58] G. Kotliar, S. Y. Savrasov, K. Haule, V. S. Oudovenko, O. Parcollet, and C. A. Marianetti, Electronic structure calculations with dynamical mean-field theory, Rev. Mod. Phys. **78**, 865 (2006).

[59] K. Haule, Exact double counting in combining the dynamical mean field theory and the density functional theory, Phys. Rev. Lett. **115**, 196403 (2015).

[60] M. Karolak, G. Ulm, T. Wehling, V. Mazurenko, A. Poteryaev, and A. Lichtenstein, Double counting in LDA + DMFT - The example of NiO, J. Electron Spectrosc. Relat. Phenom. **181**, 11 (2010).

[61] A. Hariki, Y. Ichinozuka, and T. Uozumi, Dynamical mean-field approach to Ni 2p x-ray photoemission spectra of NiO: A role of antiferromagnetic ordering, J. Phys. Soc. Jpn. **82**, 043710 (2013).

[62] T. Yamaguchi, M. Furo, Y. Sakai, T. Nishikubo, H. Hojo, M. Azuma, K. Oka, D. Mori, Y. Inaguma, M. Mizumaki, K. Yamamoto, J. Kuneš, T. Mizokawa, and A. Hariki, Mechanism of intermetallic charge transfer and bond disproportionation in $BiNiO_3$ and $PbNiO_3$ revealed by hard x-ray photoemission spectroscopy, Phys. Rev. B **109**, 205131 (2024).

[63] The probing depth in photoemission experiments depends on the inelastic mean free path of the outgoing photoelectrons, which scales with kinetic energy [$E_K \approx (h\nu - 850)$ eV for Ni $2p$ photoelectrons], and are roughly estimated to be on the order of 15, 10, and 1 nm [69,91] for 10, 6.5, and 1.2 keV photons, respectively.

[64] M. B. Trzhaskovskaya and V. G. Yarzhemsky, Dirac–Fock photoionization parameters for HAXPES applications, At. Data Nucl. Data Tables **119**, 99 (2018).

[65] M. Taguchi, A. Chainani, K. Horiba, Y. Takata, M. Yabashi, K. Tamasaku, Y. Nishino, D. Miwa, T. Ishikawa, T. Takeuchi, K. Yamamoto, M. Matsunami, S. Shin, T. Yokoya, E. Ikenaga, K. Kobayashi, T. Mochiku, K. Hirata, J. Hori, K. Ishii, F. Nakamura, and T. Suzuki, Evidence for suppressed screening on the surface of high temperature $La_{2-x}Sr_xCuO_4$ and $Nd_{2-x}Ce_xCuO_4$ superconductors, Phys. Rev. Lett. **95**, 177002 (2005).

[66] S. Suga and A. Sekiyama, Soft x-ray ARPES and Fermiology of strongly correlated electron systems and PES by hard X-ray and extremely low energy photons, J. Electron Spectrosc. Relat. Phenom. **181**, 48 (2010).

[67] G. Panaccione and K. Kobayashi, Hard x-ray photoemission spectroscopy: Variable depth analysis of bulk, surface and interface electronic properties, Surf. Sci. **606**, 125 (2012).

[68] C. N. Veenstra, Z.-H. Zhu, B. Ludbrook, M. Capsoni, G. Levy, A. Nicolaou, J. A. Rosen, R. Comin, S. Kittaka, Y. Maeno, I. S. Elfimov, and A. Damascelli, Determining the surface-to-bulk progression in the normal-state electronic structure of Sr_2RuO_4 by angle-resolved photoemission and density functional theory, Phys. Rev. Lett. **110**, 097004 (2013).

[69] *Hard X-ray Photoelectron Spectroscopy (HAXPES)* edited by J. C. Woicik, *Springer Series in Surface Sciences* (Springer International Publishing, Cham, 2016).

[70] D. Takegami, A. Tanaka, S. Agrestini, Z. Hu, J. Weinen, M. Rotter, C. Schüßler-Langeheine, T. Willers, T. C. Koethe, T. Lorenz, Y. F. Liao, K. D. Tsuei, H.-J. Lin, C. T. Chen, and L. H. Tjeng, Paramagnetic $LaCoO_3$: A highly inhomogeneous mixed spin-state system, Phys. Rev. X **13**, 011037 (2023).

[71] D. Takegami, M. Nakamura, A. Melendez-Sans, K. Fujinuma, R. Nakamura, M. Yoshimura, K.-D. Tsuei, A. Tanaka, M. Gen, Y. Tokunaga, S. Ishiwata, and T. Mizokawa, Negative charge-transfer energy in $SrFeO_3$ revisited with hard x-ray photoemission spectroscopy, Phys. Rev. B **109**, 235138 (2024).

[72] M. Winder, A. Hariki, and J. Kuneš, X-ray spectroscopy of the rare-earth nickelate $LuNiO_3$: LDA+DMFT study, Phys. Rev. B **102**, 085155 (2020).

[73] J. Zaanen, G. A. Sawatzky, and J. W. Allen, Band gaps and electronic structure of transition-metal compounds, Phys. Rev. Lett. **55**, 418 (1985).

[74] Similar results apply for the Ni valencies in $NdNiO_3$, more directly related to the $Nd_3Ni_2O_7$, as shown from the similarities of the Ni L_3-edge x-ray absorption spectrum between $LuNiO_3$ and $NdNiO_3$ [4,72].

[75] T. Mizokawa, A. Fujimori, T. Arima, Y. Tokura, N. Mōri, and J. Akimitsu, Electronic structure of $PrNiO_3$ studied by photoemission and x-ray-absorption spectroscopy: Band gap and orbital ordering, Phys. Rev. B **52**, 13865 (1995).

[76] R. J. Green and G. A. Sawatzky, Negative charge transfer energy in correlated compounds, J. Phys. Soc. Jpn. **93**, 121007 (2024).

[77] We performed additional LDA+DMFT calculations for the experimental structure, allowing for a checkerboard pattern of CD as observed in $RNiO_3$.

[78] H. Park, A. J. Millis, and C. A. Marianetti, Site-selective mott transition in rare-earth-element nickelates, Phys. Rev. Lett. **109**, 156402 (2012).

[79] A. B. Georgescu, O. E. Peil, A. S. Disa, A. Georges, and A. J. Millis, Disentangling lattice and electronic contributions to the metal-insulator transition from bulk vs. layer confined $RNiO_3$, Proc. Natl. Acad. Sci. USA **116**, 14434 (2019).

[80] J. Ruppen, J. Teyssier, O. E. Peil, S. Catalano, M. Gibert, J. Mravlje, J.-M. Triscone, A. Georges, and D. van der Marel, Optical spectroscopy and the nature of the insulating state of rare-earth nickelates, Phys. Rev. B **92**, 155145 (2015).

[81] O. E. Peil, A. Hampel, C. Ederer, and A. Georges, Mechanism and control parameters of the coupled structural and metal-insulator transition in nickelates, Phys. Rev. B **99**, 245127 (2019).

[82] S. B. Lee, R. Chen, and L. Balents, Landau theory of charge and spin ordering in the nickelates, Phys. Rev. Lett. **106**, 016405 (2011).

[83] B. Geisler, J. J. Hamlin, G. R. Stewart, R. G. Hennig, and P. J. Hirschfeld, Structural transitions, octahedral rotations, and electronic properties of $A_3Ni_2O_7$ rare-earth nickelates under high pressure, npj Quantum Mater. **9**, 38 (2024).

[84] J. Yang, H. Sun, X. Hu, Y. Xie, T. Miao, H. Luo, H. Chen, B. Liang, W. Zhu, G. Qu, C.-Q. Chen, M. Huo, Y. Huang, S. Zhang, F. Zhang, F. Yang, Z. Wang, Q. Peng, H. Mao, G. Liu, Z. Xu, T. Qian, D.-X. Yao, M. Wang, L. Zhao, and X. J. Zhou, Orbital-dependent electron correlation in double-layer nickelate $La_3Ni_2O_7$, Nat. Commun. **15**, 4373 (2024).

[85] H. Sakakibara, N. Kitamine, M. Ochi, and K. Kuroki, Possible high T_c superconductivity in $La_3Ni_2O_7$ under high pressure through manifestation of a nearly half-filled bilayer Hubbard model, Phys. Rev. Lett. **132**, 106002 (2024).

[86] F. Lechermann, J. Gondolf, S. Bötzel, and I. M. Eremin, Electronic correlations and superconducting instability in $La_3Ni_2O_7$ under high pressure, Phys. Rev. B **108**, L201121 (2023).

[87] Y. Cao and Y.-F. Yang, Flat bands promoted by Hund's rule coupling in the candidate double-layer high-temperature superconductor $La_3Ni_2O_7$ under high pressure, Phys. Rev. B **109**, L081105 (2024).

[88] Z. Ouyang, J.-M. Wang, J.-X. Wang, R.-Q. He, L. Huang, and Z.-Y. Lu, Hund electronic correlation in $La_3Ni_2O_7$ under high pressure, Phys. Rev. B **109**, 115114 (2024).

[89] A. Hariki, A. Hausoel, G. Sangiovanni, and J. Kuneš, DFT+DMFT study on soft moment magnetism and covalent bonding in $srru_2o_6$, Phys. Rev. B **96**, 155135 (2017).

[90] C. Watzenböck, M. Edelmann, D. Springer, G. Sangiovanni, and A. Toschi, Characteristic timescales of the local moment dynamics in Hund's metals, Phys. Rev. Lett. **125**, 086402 (2020).

[91] S. Tanuma, C. J. Powell, and D. R. Penn, Calculations of electron inelastic mean free paths. IX. Data for 41 elemental solids over the 50 eV to 30 keV range, Surf. Interface Anal. **43**, 689 (2011).